PNAS RESEARCH ARTICLE | CELL BIOLOGY OPEN ACCESS

Downregulation of apoptotic repressor *AVEN* exacerbates cardiac injury after myocardial infarction

Peng Yu[a,1], Shuai Song[b,c,1], Xiaokai Zhang[b,c,1], Shujun Cui[a], Gang Wei[a], Zihang Huang[b,c], Linqi Zeng[b,c], Ting Ni[a,d,e,f,2], and Aijun Sun[a,b,c,f,2]

Edited by James Manley, Columbia University, New York, NY; received February 12, 2023; accepted September 6, 2023

Myocardial infarction (MI) is a leading cause of heart failure (HF), associated with morbidity and mortality worldwide. As an essential part of gene expression regulation, the role of alternative polyadenylation (APA) in post-MI HF remains elusive. Here, we revealed a global, APA-mediated, 3′ untranslated region (3′ UTR)-lengthening pattern in both human and murine post-MI HF samples. Furthermore, the 3′ UTR of apoptotic repressor gene, *AVEN*, is lengthened after MI, contributing to its downregulation. *AVEN* knockdown increased cardiomyocyte apoptosis, whereas restoration of *AVEN* expression substantially improved cardiac function. Mechanistically, *AVEN* 3′ UTR lengthening provides additional binding sites for miR-30b-5p and miR-30c-5p, thus reducing AVEN expression. Additionally, *PABPN1* (poly(A)-binding protein 1) was identified as a potential regulator of *AVEN* 3′ UTR lengthening after MI. Altogether, our findings revealed APA as a unique mechanism regulating cardiac injury in response to MI and also indicated that the APA-regulated gene, *AVEN*, holds great potential as a critical therapeutic target for treating post-MI HF.

alternative polyadenylation | myocardial infarction | AVEN | apoptosis

Myocardial infarction (MI) is a severe clinical condition caused by coronary artery thrombotic occlusion that is associated with rising global morbidity and mortality (1). Despite improved reperfusion strategies and other therapies, patients often develop heart failure (HF) after MI due to progressive cell death and adverse cardiac remodeling (2). Therefore, it is important to uncover the mechanisms underlying this adverse cardiac remodeling and explore novel therapeutic strategies for treating post-MI HF.

The precise regulation of gene expression is required for normal cardiac function. Likewise, dysregulated gene expression always underlies the pathophysiology of cardiovascular diseases, such as HF (3, 4). Transcriptional regulation has been increasingly studied in cardiac development and HF pathophysiology (3, 5). Alternative polyadenylation (APA) is a widespread phenomenon in diverse species, serving as an important contributor to transcriptome diversity (6). Over 70% of mammalian protein-coding genes harbor multiple polyadenylation (poly(A)) sites, leading to the formation of distinct 3′ end messenger RNA (mRNA) isoforms (7, 8). APA in the coding region typically changes the C-terminus of a protein (9), and APA in the 3′ untranslated region (3′ UTR-APA) produces transcripts encoding the same protein but with different 3′ UTRs lengths (10). This 3′ UTR-APA can considerably affect gene expression in various ways, including mRNA stability (11, 12), mRNA translation (13), and subcellular localization of mRNA and proteins (14–16). Increasing studies have shown that the lengthening or shortening of the 3′ UTR can act as a global gene regulatory network for diverse physiological and pathological processes, including cell proliferation (12, 17), cell senescence (18), embryonic development (19), the immune response (20), and carcinogenesis (21, 22). Recently, several studies have reported that APA-mediated alterations in 3′ UTR length play important roles in the regulation of hypertrophic HF (23, 24). However, the role of APA in ischemic HF remains unknown.

Here, we discovered a global 3′ UTR-lengthening pattern after MI by analyzing RNA-seq data of samples from ischemic cardiomyopathy (ICM) patients and a murine model of MI. We demonstrated that the APA-mediated 3′ UTR lengthening contributes to downregulation of apoptosis and caspase activation inhibitor (*AVEN*). *AVEN* knockdown increases cardiomyocyte apoptosis, whereas *AVEN* overexpression attenuates cardiomyocyte apoptosis and cardiac dysfunction in mice after MI. The lengthening of *AVEN* 3′ UTR provides additional binding sites for miR-30b-5p/miR-30c-5p, thus reducing AVEN protein production. Furthermore, we identified PABPN1 (poly(A)-binding protein 1) as a potential regulator of *AVEN* 3′ UTR lengthening after MI. Our study demonstrates that APA regulates cardiac injury after MI and further suggests targeting the APA-regulated gene, *AVEN,* as a critical therapeutic approach for treating post-MI HF.

Significance

Myocardial infarction (MI) is a severe clinical condition with progressive cell death and adverse cardiac remodeling. The dynamics and roles of alternative polyadenylation (APA) after MI remain unclear. Here, we reveal a global 3′ UTR (3′ untranslated region) lengthening pattern in both human failing hearts and a mouse model of MI. APA-mediated 3′ UTR lengthening contributes to downregulation of *AVEN*. *AVEN* overexpression markedly attenuates cardiomyocyte apoptosis and cardiac dysfunction in mice after MI. *AVEN* 3′ UTR lengthening provides additional binding sites for miR-30b-5p/miR-30c-5p, thus reducing AVEN protein production. Altogether, our data reveal APA as an important mechanism for gene regulation after MI and also indicates AVEN as a potential therapeutic target against cardiac injury and dysfunction after MI.

Author contributions: P.Y., T.N., and A.S. designed research; P.Y., S.S., X.Z., S.C., Z.H., and L.Z. performed research; P.Y., S.S., and X.Z. analyzed data; and P.Y., X.Z., S.C., G.W., T.N., and A.S. wrote the paper.

The authors declare no competing interest.

This article is a PNAS Direct Submission.

[1]P.Y., S.S., and X.Z. contributed equally to this work.

[2]To whom correspondence may be addressed. Email: tingni@fudan.edu.cn or sun.aijun@zs-hospital.sh.cn.

This article contains supporting information online at https://www.pnas.org/lookup/suppl/doi:10.1073/pnas.2302482120/-/DCSupplemental.

Published October 10, 2023.

Results

Global 3′ UTR Lengthening Occurred in Both Human ICM and a Murine Model of MI. A published RNA-seq dataset (GSE116250) was analyzed to systematically investigate the global APA landscape in post-MI HF. This dataset consisted of 13 ICM and 14 non-failing (NF) left ventricular (LV) control samples (25). A well-established and widely used computational algorithm, dynamic analysis of APA from RNA-seq (DaPars) (21), was used to identify dynamic alterations in APA between the ICM and control samples. The difference in 3′ UTR length between the samples was quantified as a change in percentage of distal poly(A) site usage index (deltaPDUI). Interestingly, an obvious APA-mediated 3′ UTR lengthening (larger PDUI value) pattern was observed in the ICM samples compared with the control samples (*SI Appendix*, Fig. S1*A*), among which 842 genes with significantly 3′ UTR lengthened and 31 genes with significantly 3′ UTR shortened (Fig. 1*A*). Two representative examples of genes with lengthened 3′ UTRs in the ICM samples compared with the control samples were high-mobility group nucleosomal binding domain 3 (*HMGN3*) and a disintegrin and metalloprotease domain 9 (*ADAM9*) (Fig. 1 *B* and *C* and *SI Appendix*, Fig. S1 *B–E*). To further verify the reliability of the DaPars-predicted poly(A) sites located within 3′ UTRs, the 40-nucleotide upstream regions of the predicted poly(A) sites were analyzed. MEME motif enrichment analysis revealed significant enrichment of the canonical poly(A) signal (AAUAAA) (26) (*SI Appendix*, Fig. S1*F*), indicating the reliability of the overall procedure.

Functional enrichment analysis was performed to characterize the biological functions associated with the differential APA genes. Gene ontology (GO) terms, including muscle contraction, muscle tissue development, and mitochondrial translation, were highly enriched in genes with 3′ UTR lengthening in the ICM samples (Fig. 1*D*). Interestingly, these genes with 3′ UTR lengthening were also highly enriched in Kyoto Encyclopedia of Genes and Genomes (KEGG) terms such as carbon metabolism, pyruvate metabolism, and citrate cycle (*SI Appendix*, Fig. S1*G*), suggesting that APA-mediated 3′ UTR lengthening may be involved in regulating different metabolic processes during ICM.

Independent RNA-seq data of human ischemic LV samples from APAatlas (27) were further analyzed to determine whether global 3′ UTR lengthening was induced by ischemia. A trend was identified, in which PDUIs increased over the duration of ischemia (*SI Appendix*, Fig. S2*A*). Specifically, 1,928 genes with 3′ UTR lengthening and 123 genes with 3′ UTR shortening were identified in samples after 20 min of ischemia compared with control samples (Fig. 1*E*). This consistency in the APA patterns of the ICM and myocardial ischemia samples suggests that APA may play a role in the regulation of gene expression in ischemic heart disease.

Next, dynamic alterations in APA-mediated 3′ UTR length were evaluated in a murine model of cardiac ischemia. Cardiac ischemia was induced in these mice by MI surgery, and subsequent analyses were performed 7 and 28 d later. RNA-seq libraries were constructed and sequenced, and the data were analyzed via the analysis pipeline described above. Consistent with our findings from the human data, the number of genes with lengthened 3′ UTRs was much larger than that of genes with shortened 3′ UTRs (1,531 vs. 92) in the mouse MI samples compared with the control sham samples (*SI Appendix*, Fig. S2 *B* and *C*). GO analysis revealed that these genes with lengthened 3′ UTRs were highly enriched for muscle cell differentiation and mitochondrial organization, which were consistent with the GO terms enriched in the human ICM samples (*SI Appendix*, Fig. S2*D*). KEGG pathway analysis also revealed that these genes were enriched with key pathways involved in the regulation of cardiac function and ischemic injury (*SI Appendix*, Fig. S2*E*). The above data suggest that global 3′ UTR lengthening is a prevalent molecular phenomenon in both human ICM and a MI murine model.

***AVEN* Was Identified as Having a Lengthened 3′ UTR and Decreased Expression in ICM.** A longer 3′ UTR region resulting from APA may promote the binding of RNA-binding proteins (RBPs) and microRNAs (miRNAs), thus influencing mRNA and/or protein abundance (11, 21). In line with this hypothesis, gene downregulation was more prevalent in the human ICM samples (56 down-regulated vs. 30 up-regulated genes), suggesting that these genes with lengthened 3′ UTRs may have a greater opportunity to downregulate their steady-state mRNA expression during ICM (*SI Appendix*, Fig. S3*A*). GO enrichment analysis on the 56 down-regulated genes showed that they were enriched in pathways related to mitochondrial respiration, electron transport chain, and cardiac muscle contraction (*SI Appendix*, Fig. S3*B*). This suggests that genes with APA changes may play a role in regulating cardiac function after MI, which warrants further investigation. This postulation remained consistent in the MI mouse model (684 down-regulated vs. 383 up-regulated genes) (*SI Appendix*, Fig. S3*C*).

To further explore whether APA-mediated 3′ UTR lengthening was a potential contributor of cardiac injury after MI or if it was only associated with it, additional screening analysis was performed to identify potential candidate genes for further functional validation studies. The screening analysis identified overlapping candidate genes with 3′ UTR lengthening in the ICM and APAatlas ischemic LV samples (Fig. 1*F*). Of these, only the down-regulated genes were chosen for further investigation. The following criteria were then used to confirm the authenticity of these APA events: RNA-seq track plot favored distal poly(A) site usage, contained a classical poly(A) signal (AAUAAA or AUUAAA), and contained poly(A) site annotation in APA databases. Five candidate genes passed these three screening steps (Fig. 2 *A–C* and *SI Appendix*, Figs. S4 and S5). The long and short 3′ UTRs (UTR-L/UTR-S) of these five candidate genes were separately cloned into the psiCHECK2 vector, and dual-luciferase reporter assays were performed to evaluate whether the longer 3′ UTRs resulted in lower protein production. Two out of the five genes exhibited reduced protein expression with the longer 3′ UTR (Fig. 2*E* and *SI Appendix*, Fig. S6 *A–E*). One of these genes was *AVEN* and the other was signal-induced proliferation-associated 1 like 2. Considering the predominant role of cardiomyocyte cell death in the pathogenesis of post-MI HF (28, 29), *AVEN* was chosen for further investigation.

The antiapoptotic protein, AVEN (30), has been shown to be involved in the regulation of multiple cancers (31, 32). However, its role in cardiovascular disease remains unknown. The use of distal poly(A) sites within *AVEN* during ICM was further confirmed. RNA-seq density plots for *AVEN* showed obvious 3′ UTR lengthening in three representative ICM samples (Fig. 2*A*). The PDUIs of these samples were significantly increased, whereas *AVEN* expression was significantly decreased compared with the NF control samples (Fig. 2 *B* and *C*). 3′ RACE experiments in human ICM samples and cell lines (AC16 and HEK293T) further validated the authenticity of *AVEN* proximal and distal poly(A) sites (Fig. 2*D* and *SI Appendix*, Fig. S7 *A–D*). To investigate how APA-induced 3′ UTR lengthening of *AVEN* contributes to gene expression changes, we evaluated the RNA degradation rate of *AVEN* transcripts containing UTR-L/UTR-Ss. After blocking transcription followed by qRT-PCR, we found that *AVEN* transcripts with a longer 3′ UTR were less stable

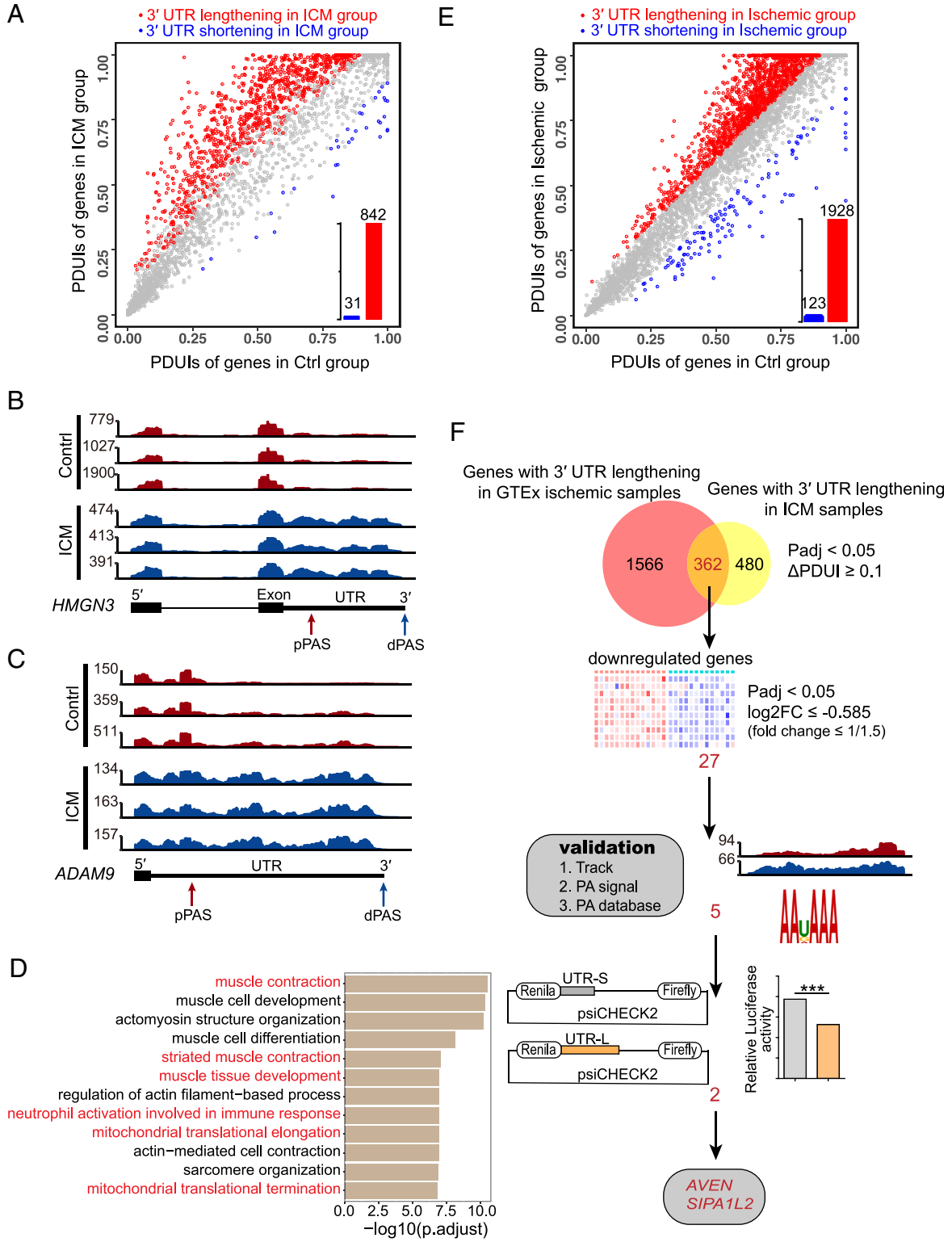

Fig. 1. Global 3′ UTR lengthening occurs in both human ICM and a murine model of MI. (*A*) Scatterplot of PDUIs showing lengthened (n = 842) or shortened (n = 31) 3′ UTRs in the ICM group compared with the control (Ctrl) group. Control, n = 14, ICM, n = 13. False discovery rate (FDR) < 0.05, absolute ΔPDUIs ≥ 0.1 between control and ICM groups are colored. (*B* and *C*) Representative RNA-seq density plots for *HMGN3* (*B*) and *ADAM9* (*C*) with 3′ UTR lengthening. Numbers on the *y* axis indicate RNA-seq read coverage. (*D*) GO Pathways significantly enriched for genes tended to use distal poly(A) sites (ΔPDUIs ≥ 0.1) in ICM group. (*E*) Scatterplot of PDUIs showing lengthened or shortened 3′ UTRs in human ischemic LV samples (ischemic group) from APAatlas using the same cutoffs as in *A*. Control, n = 112, ischemic group, n = 34. (*F*) Flowchart of the screening process for candidate genes. Briefly, we carried out a four-step screening strategy. First, overlapped (n = 362) genes with 3′ UTR lengthening (adjusted *P*-value [Padj] < 0.05, ΔPDUIs ≥ 0.1) in the ICM and APAatlas ischemic LV samples were chosen. Second, we focused on the down-regulated genes (Padj < 0.05, log2FC ≤ −0.585 [fold change ≤ 1/1.5]). Third, RNA-seq track plot and poly(A) signal of these genes and the annotated poly(A) site in APA databases were further confirmed. Finally, dual-luciferase reporter assays were performed to evaluate if the longer 3′ UTRs resulted in lower protein production.

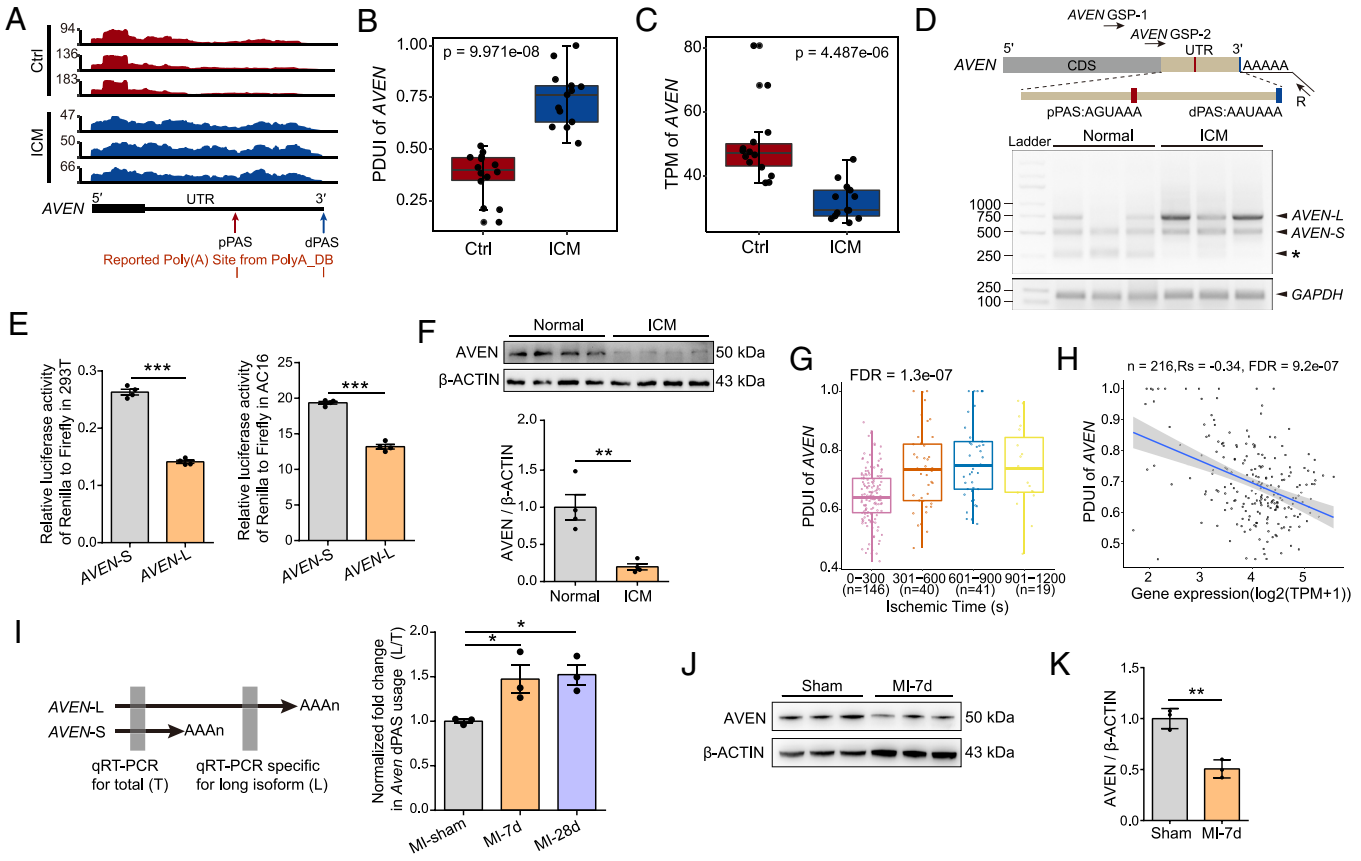

Fig. 2. APA-mediated *AVEN* 3′ UTR lengthening reduces AVEN protein production in ICM. (*A*) Representative RNA-seq density plots for *AVEN* 3′ UTR lengthening in ICM samples. Numbers on the *y* axis indicate RNA-seq read coverage. (*B* and *C*) Graph showing significantly increased PDUIs and decreased TPMs for *AVEN* in ICM samples. PDUI, percentage of distal poly(A) site usage index. TPM, transcripts per kilobase of exon model per million mapped reads. The *P*-value was calculated based on a two-sided Wilcoxon rank-sum test; Control, n = 14, ICM, n = 13. (*D*, *Top*) schematic for 3′ RACE of *AVEN*. Forward primers: *AVEN* GSP-1, *AVEN* GSP-2; reverse primer: R. (*Bottom*) Agarose gel electrophoresis for 3′ RACE using primer pairs in the human ICM samples and healthy control (Normal) samples. *GAPDH* serves as the internal control. *AVEN*-L and *AVEN*-S indicate transcript with longer or shorter 3′ UTR, respectively. The asterisk (*) indicates a potential RACE hetero-band (Sanger sequencing shown in *SI Appendix*, Fig.S7*B*) located above the band at 250 bp. (*E*) Luciferase activity from a reporter system containing the shortened (*AVEN*-S) or lengthened (*AVEN*-L) *AVEN* 3′ UTR in HEK293T (*Left*) and AC16 (*Right*) cells. (***) *P*-value < 0.001, two-tailed Student's *t* test; n = 4 for each group. (*F*) Western blot of AVEN expression in control and ICM samples. Internal control, β-ACTIN. (**) *P*-value < 0.01, two-tailed Student's *t* test; n = 4 for each group. (*G*) *AVEN* PDUI showing a significant increase over the duration of ischemia in LV samples from APAatlas. (*H*) *AVEN* PDUI negatively correlates with its gene expression. (*I*) qRT-PCR showing increased *Aven* distal poly(A) site usage (ratio between long/total isoform, L/T) in mice after MI (MI-7d, n = 3; MI-28d, n = 3) compared with the sham group (MI-sham, n = 3). (*) *P*-value < 0.05, two-tailed Student's *t* test. *Left* panel showed diagram of the primer pair design, as highlighted in gray rectangle. *Right* panel showed qRT-PCR result. (*J*) Western blot of AVEN expression in LV samples from sham (n = 3) and MI (n = 3) mice. Internal control, β-ACTIN. (*K*) Quantification of (*J*), (**) *P*-value < 0.01, two-tailed Student's *t* test; n = 3.

than those with a shorter 3′ UTR (*SI Appendix*, Fig. S7*E*). A dual-luciferase reporter assay was next conducted in HEK293T cells and human cardiomyocyte cell line AC16 to evaluate the effects of *AVEN* 3′ UTR lengthening on protein production. The longer *AVEN* 3′ UTR (*AVEN*-L) resulted in significantly reduced luciferase activity, indicating that the increased length reduced its expression (Fig. 2*E*). We then constructed *AVEN* coding sequence with long or short 3′ UTRs downstream of enhanced green fluorescent protein (EGFP) and found that cells transfected with shorter 3′ UTR of *AVEN* have higher green fluorescence than that of longer 3′ UTR (*SI Appendix*, Fig. S7*F*). Western blot also confirmed that shorter 3′ UTR generates more protein than the longer one (*SI Appendix*, Fig. S7*G*). Consistently, reduced AVEN protein levels were detected in the human ICM samples compared with the healthy control samples (Fig. 2*F*). This finding was verified using the larger ischemic sample size from APAatlas. *AVEN* PDUIs significantly increased over the duration of ischemia (Fig. 2*G*). Furthermore, *AVEN* expression was negatively correlated with its PDUI value (Fig. 2*H*). These data support the high correlation between *AVEN* 3′ UTR lengthening and ischemic conditions in humans.

Aven 3′ UTR lengthening was further validated in the MI mouse model by qRT-PCR (Fig. 2*I*). AVEN protein levels were also significantly decreased in these mice (Fig. 2 *J* and *K*). Altogether, *AVEN* 3′ UTR lengthening contributed to the down-regulation of its protein levels in both human ICM and post-MI mouse cardiac samples.

Reduced AVEN Expression Increased Cardiomyocyte Apoptosis In Vitro. To verify whether *AVEN* downregulation regulates cardiomyocyte apoptosis, *AVEN* was knocked down with two short hairpin RNAs (shRNAs) in human AC16 cells (Fig. 3*A*). *AVEN* knockdown significantly decreased cell viability (Fig. 3*B*) and increased pro-apoptotic BCL-2 (B-cell lymphoma 2)-associated X (BAX) protein levels (Fig. 3*C*). Flow cytometry revealed that *AVEN* knockdown significantly enhanced apoptosis (Fig. 3 *D* and *E*). Additionally, *AVEN* knockdown induced the activity of caspase-3, the primary executor of apoptosis (Fig. 3*F*). Finally, terminal deoxynucleotidyl-transferase-mediated dUTP nick-end labeling (TUNEL) staining revealed that *AVEN* knockdown increased the number of TUNEL$^+$ AC16 cells, indicating increased apoptosis (Fig. 3 *G* and *H*). Consistent with these findings in AC16 cells,

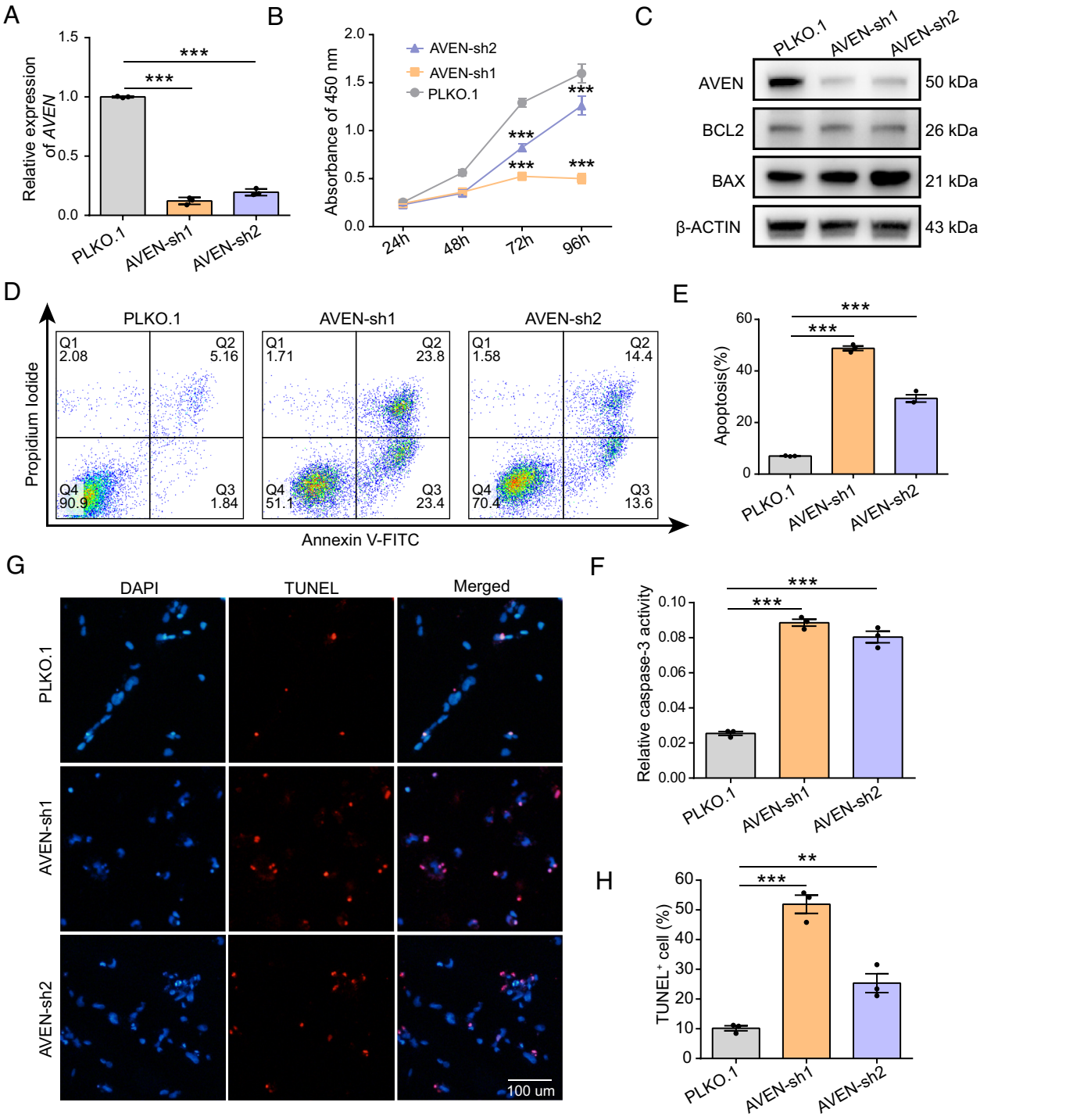

Fig. 3. AVEN downregulation induces apoptosis in AC16 cells. (*A*) Validation of *AVEN* knockdown by two shRNAs (*AVEN*-sh1 and *AVEN*-sh2) in AC16 cells. (***) *P*-value < 0.001, two-tailed Student's *t* test; n = 3 for each group. (*B*) CCK-8 assay showing cell viability of AVEN-knockdown (AVEN-KD) and control AC16 cells. (***) *P*-value < 0.001, two-tailed Student's *t* test; n = 3 for each group. (*C*) Western blot of AVEN, BAX and BCL2 protein levels before and after AVEN knockdown in AC16 cells. Internal control, β-ACTIN. (*D*) Flow cytometry analysis using annexin V and propidium iodide double-staining to assess apoptosis in AVEN-KD AC16 cells. (*E*) Quantification of *D*. (***) *P*-value < 0.001, two-tailed Student's *t* test; n = 3 for each group. (*F*) Caspase-3 activity indicating apoptosis after AVEN knockdown in AC16 cells. (***) *P*-value < 0.001, two-tailed Student's *t* test; n = 3 for each group. (*G*) TUNEL and DAPI staining before (PLKO.1) and after AVEN knockdown in AC16 cells. (Scale bar, 100 μm.) (*H*) Percentage of TUNEL$^+$ AC16 cells. (***) *P*-value < 0.001, two-tailed Student's *t* test; n = 3 for each group.

AVEN exhibited an antiapoptotic function in HEK293T cells (*SI Appendix*, Fig. S8), suggesting that AVEN function remains consistent within different cell types.

Next, the effects of *AVEN* knockdown by small interfering RNAs (siRNAs) and overexpression by adenovirus were assessed in primary neonatal rat ventricular myocytes (NRVMs). Consistent with the results in AC16 cells, the BAX/BCL-2 ratio was increased after *AVEN* knockdown and the expression of caspase-3 was also decreased (Fig. 4 *A*–*C*), indicating activation of apoptotic pathways. TUNEL staining further showed significantly more TUNEL$^+$ NRVMs after *AVEN* knockdown (Fig. 4 *D* and *E*). In contrast, *AVEN* overexpression significantly decreased the BAX/BCL-2 ratio (Fig. 4 *F* and *G*), indicating the antiapoptotic effect of AVEN. Altogether, these findings demonstrate an

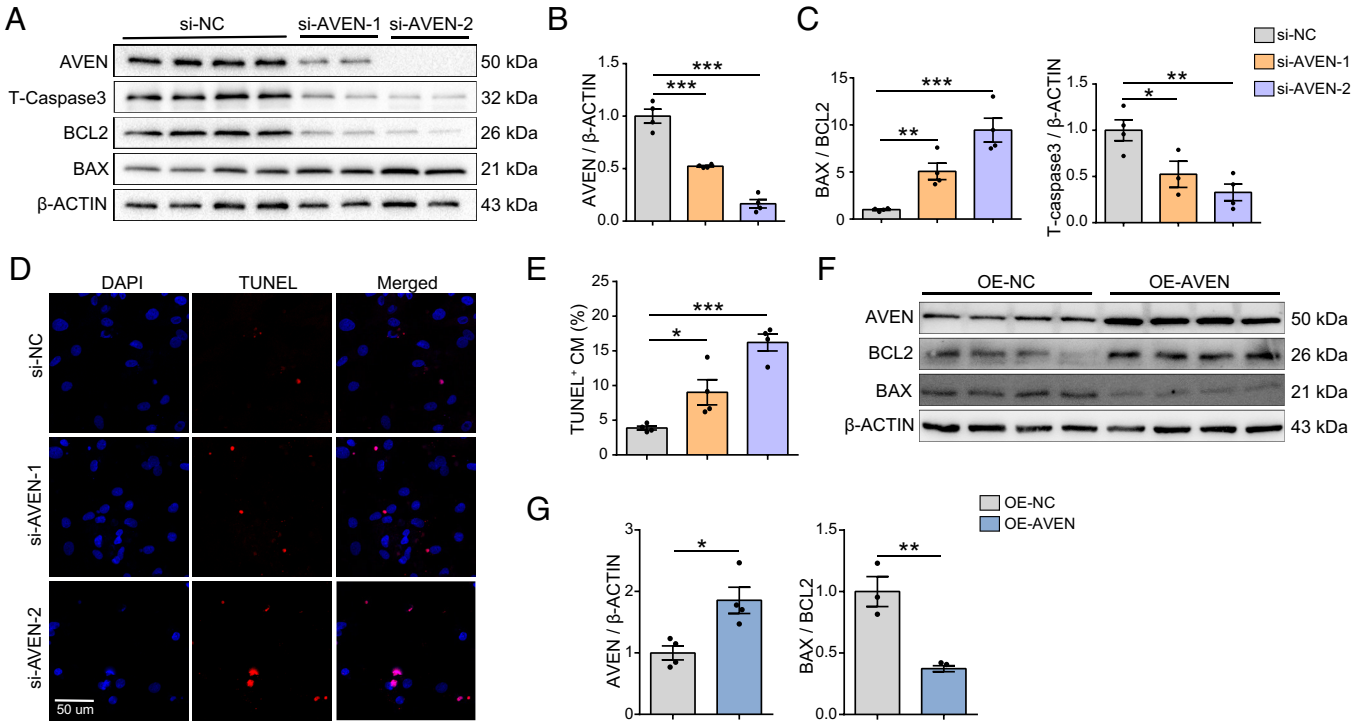

Fig. 4. AVEN regulates apoptosis in NRVMs. (*A*) Western blot of AVEN, BAX, BCL2, and T-Caspase-3 protein levels before (si-NC) and after AVEN knockdown (si-AVEN-1 and si-AVEN-2) in NRVMs. Internal control, β-ACTIN. (*B* and *C*) Quantification of *A*. (∗) *P*-value < 0.05, (∗∗) *P*-value < 0.01, (∗∗∗) *P*-value < 0.001, two-tailed Student's *t* test; n = 4 for each group. (*D*) Apoptosis indicated by TUNEL and DAPI staining before (si-NC) and after AVEN knockdown (si-AVEN-1 and si-AVEN-2) in NRVMs. (Scale bar, 50 μm.) (*E*) Percentage of TUNEL$^+$ cardiomyocytes. (∗) *P*-value < 0.05, (∗∗∗) *P*-value < 0.001, two-tailed Student's *t* test; n = 4 for each group. (*F*) Western blot of AVEN, BAX, and BCL-2 protein levels before (OE-NC) and after AVEN overexpression (OE-AVEN) in NRVMs. Internal control, β-ACTIN. (*G*) Quantification of (*F*). (∗) *P*-value < 0.05, (∗∗) *P*-value < 0.01, two-tailed Student's *t* test; n = 4 for each group.

evolutionarily conserved mechanism, in which *AVEN* downregulation leads to cardiomyocyte apoptosis.

AVEN Overexpression Attenuated Cardiomyocyte Apoptosis and Cardiac Dysfunction in Mice after MI. To further determine the in vivo effects of *AVEN* overexpression, 8-wk-old male mice were injected with AAV9-CTNT-m-Aven-3xflag-EGFP (AAV-AVEN) or AAV9-CTNT-EGFP [AAV-NC (negative control)] control virus via the tail vein 3 wk before MI surgery. Tissue and cardiac function analyses were performed 7 and 28 d after MI (Fig. 5*A*). AVEN overexpression was validated by qRT-PCR (*SI Appendix*, Fig. S9*A*) and Western blot (Fig. 5 *B* and *C*). Echocardiographic analysis revealed a drastic decline in the overall LV ejection fraction (EF) and fractional shortening (FS) of the AAV-NC mice 7 and 28 d post-MI. However, contractile function was significantly preserved in the AAV-AVEN mice (Fig. 5 *D*–*F* and *SI Appendix*, Fig. S9 *B* and *C* and Tables S4 and S5). Moreover, Masson's trichrome staining demonstrated that AAV9-AVEN mice exhibited markedly reduced MI scar sizes compared with those of AAV-NC mice 7 and 28 d post-MI (Fig. 5 *G* and *H* and *SI Appendix*, Fig. S9 *D* and *E*). These phenotypic characteristics were consistent with a decreased BAX/BCL-2 ratio in the AAV-AVEN mice (Fig. 5 *I* and *J* and *SI Appendix*, Fig. S9 *F* and *G*). Moreover, *AVEN* overexpression decreased the mRNA levels of atrial natriuretic peptide (*Anp*) and brain natriuretic peptide (*Bnp*) 28 d post-MI (Fig. 5*K*). These data suggest that *AVEN* overexpression may be an effective strategy to protect against MI-induced cardiomyocyte apoptosis and cardiac dysfunction.

The Reduced Expression that Occurred with *AVEN* 3′ UTR Lengthening Was due to miR-30b-5p/miR-30c-5p. Because miRNAs repress gene expression upon binding to 3′ UTRs, analysis was performed to evaluate whether miRNAs were responsible for the reduced expression that occurred with *AVEN* 3′ UTR lengthening. Two bioinformatics tools (TargetScan, miRDB) were used to identify five miRNAs that bind to the lengthened *AVEN* 3′ UTR and subsequently decrease translation and/or promote RNA degradation (*SI Appendix*, Fig. S10 *A* and *B*). Two of these miRNAs were ruled out because they had very low expression in human myocardial samples and two cell lines (AC16, HEK293T) (*SI Appendix*, Fig. S10 *C* and *D*); thus, three candidate miRNAs (miR-30b-5p, miR-30c-5p, and miR-15a-5p) remained. Mimics of these three miRNAs and a NC were separately transfected into AC16 cells to validate their repressive effects on *AVEN* expression. Overexpression of miRNA-30b-5p or miRNA-30c-5p significantly decreased *AVEN* mRNA levels, but this did not occur with miR-15a-5p overexpression (Fig. 6 *A*–*D* and *SI Appendix*, Fig. S10 *E* and *F*).

To further verify the effects of miR-30b-5p and miR-30c-5p on the expression of *AVEN* with its lengthened 3′ UTR, a dual-luciferase reporter assay was performed in both AC16 and HEK293T cells after cotransfection with *AVEN*-L and either the miR-30b-5p/miR-30c-5p mimic or NC. Significantly reduced luciferase activity was observed with miR-30b-5p/miR-30c-5p overexpression in both cell lines (Fig. 6*E*). These results indicate that miR-30b-5p and miRNA-30c-5p may play important roles in the downregulation of *AVEN*.

Next, the predicted miR-30b-5p/miR-30c-5p binding sequence in *AVEN*-L was mutated (termed *AVEN*-M) to verify the direct binding of miR-30b-5p/miR-30c-5p (Fig. 6*F*). The dual-luciferase reporter assay demonstrated that *AVEN*-M increased the relative luciferase activity even with miR-30b-5p/miR-30c-5p overexpression (Fig. 6 *G* and *H*). Altogether, these data demonstrate

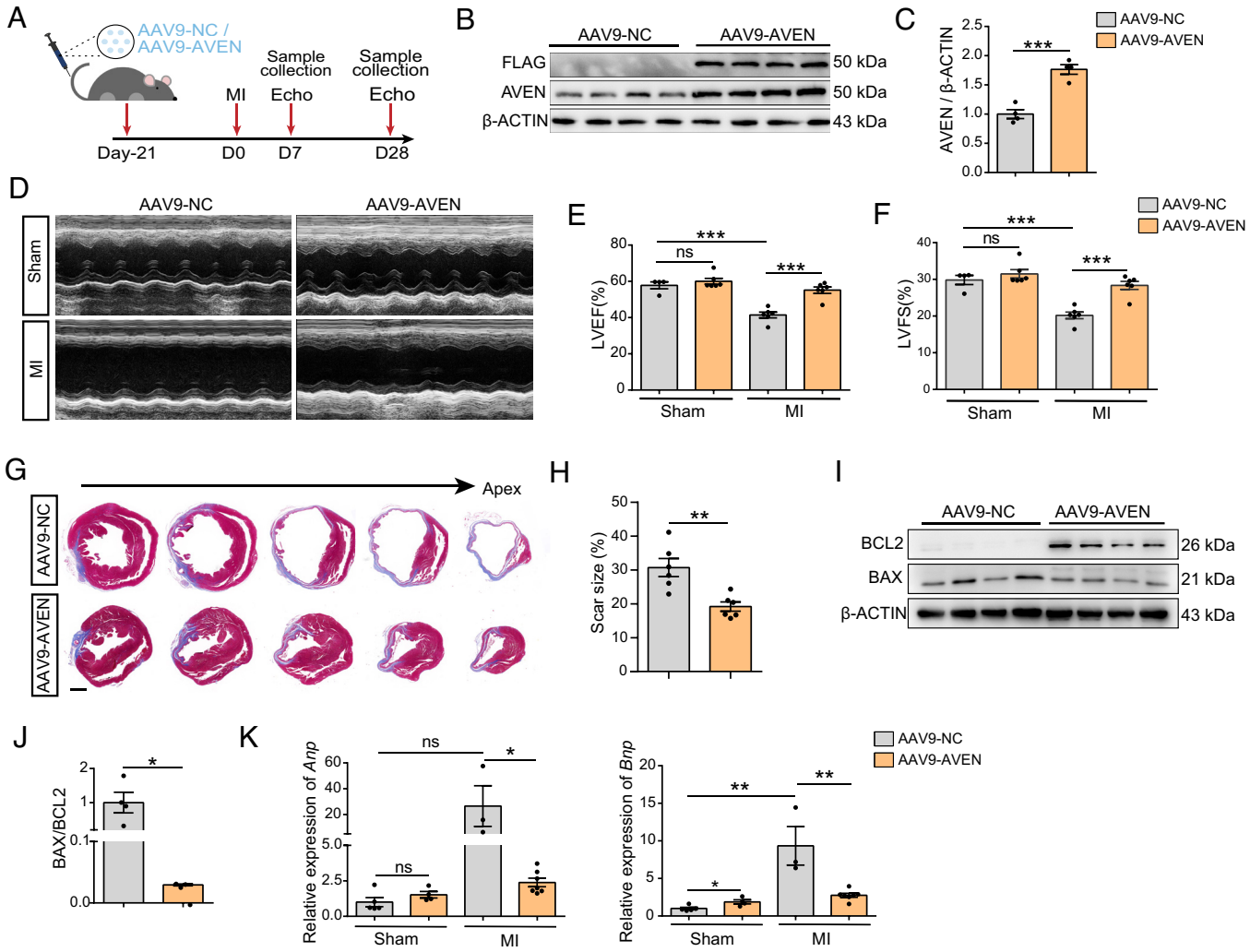

Fig. 5. AVEN overexpression attenuates MI-induced apoptosis and HF. (*A*) Schematic illustration of experimental design. (*B*) Western blot of FLAG and AVEN protein levels in the hearts of mice with AVEN overexpression (AAV9-AVEN, n = 4) and control mice (AAV9-NC, n = 4). (*C*) Quantification of *B*. (***) *P*-value < 0.001, two-tailed Student's *t* test; n = 4 for each group. (*D*) Echocardiographic analysis of mice with AVEN overexpression and control mice 28 d after MI or sham surgery. (*E* and *F*) Echocardiographic parameters of *D*. (LVEF and LVFS, n = 4, 6, 6, and 6, respectively). (**) *P*-value < 0.01, (***) *P*-value < 0.001, two-tailed Student's *t* test. (*G* and *H*) Trichrome staining of serial sections of mice heart 28 d after MI. AAV-AVEN injection reduced the scar size (the blue collagen region) of MI heart, (scale bar, 1 mm.) Average scar sizes calculated by ImageJ (*H*, n = 6 per group). (**) *P*-value < 0.01, two-tailed Student's *t* test. (*I*) Western blot of BAX and BCL-2 protein levels in hearts from control mice and mice with *AVEN* overexpression 28 d after MI surgery. (*J*) Quantification of *I*. (*) *P*-value < 0.05, two-tailed Student's *t* test; n = 4 for each group. (*K*) qRT-PCR analysis of atrial natriuretic peptide (*Anp*) and brain natriuretic peptide (*Bnp*) expression in hearts from control mice and mice with *AVEN* overexpression 28 d after MI or sham surgery (n = 5, 4, 3, and 7, respectively). LVEF, left ventricular ejection fraction; LVFS, left ventricular fraction shortening; MI, myocardial infarction; ns, not significant.

miR-30b-5p and miR-30c-5p as key regulators that bind to the lengthened *AVEN* 3′ UTR to reduce *AVEN* expression.

Several CP (Cleavage and Polyadenylation) Factors Were Up-Regulated after MI. The potential mechanisms governing the APA dynamics after MI were next investigated. Given the complexity and precision of the regulation during 3′ end processing, even small changes in the expression of core CP factors may affect 3′ end processing and alter the ratio of 3′ UTR isoforms (6, 10, 33). Interestingly, the mRNA expression of most core CP factors was up-regulated in the MI mouse model (Fig. 7*A*). Among these factors, nudix hydrolase 21 (NUDT21), CP-specific factor 6 (CPSF6), nuclear PABPN1, which have all been reported to promote 3′ UTR lengthening, were significantly up-regulated in the MI mouse model (CP factor protein phosphatase 1 catalytic subunit beta [PPP1CB] was used as the NC) (Fig. 7*B*). Serine/arginine-rich splicing factor 3 (SRSF3) is an RBP that regulates global alternative splicing and APA (34), and our previous work also demonstrated that it regulates global APA by promoting 3′ UTR lengthening during cellular senescence (35). SRSF3 is also up-regulated in the MI mouse model (Fig. 7*B* and *SI Appendix*, Fig. S11*A*). The upregulation of these four CP factors was further confirmed in human ICM samples based on the published RNA-seq dataset (Fig. 7*C*).

A recent global study in HEK293 cells has suggested that *CPSF6* knockdown induces global 3′ UTR shortening (33, 36). Analysis of this published RNA-seq data identified 1,814 genes with shortened 3′ UTRs after *CPSF6* knockdown among which 156 genes from our analysis have lengthened 3′ UTRs in ICM samples where *CPSF6* is up-regulated (Fig. 7 *D* and *E*; *P* - value = 7.16e−19 using Fisher's exact test). Similarly, 1,019 genes with shortened 3′ UTRs were identified upon *NUDT21* knockdown in HEK293 cells among which 117 genes have lengthened 3′ UTRs in ICM samples where *NUDT21* is up-regulated (*SI Appendix*, Fig. S11 *B* and *C*; *P* - value = 1.20e−24 using Fisher's exact test). *SRSF3* knockdown in human umbilical vein endothelial cell (HUVEC) induced global 3′ UTR shortening and these genes significantly overlapped with those with 3′ UTR lengthening in the ICM samples (*SI Appendix*, Fig. S11 *D* and *E*). These findings further indicate that the

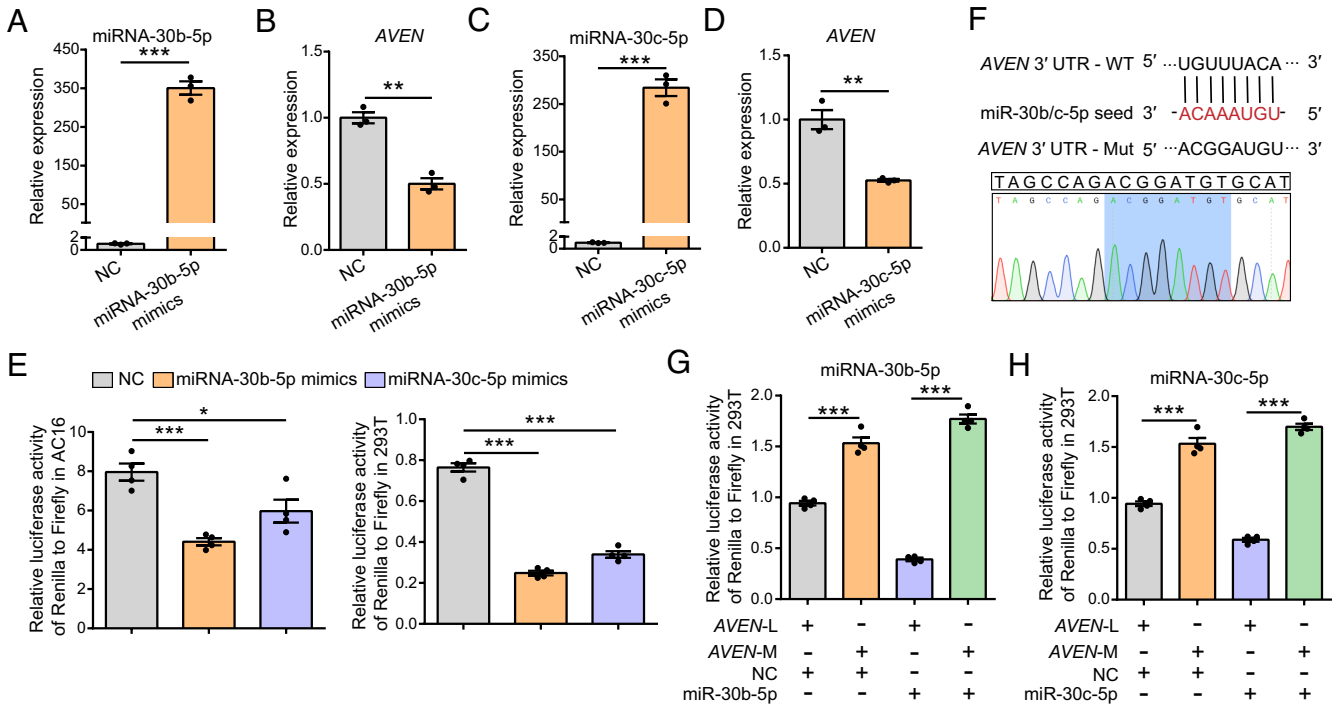

Fig. 6. The 3′ UTR lengthening-induced reduction in *AVEN* expression is due to miR-30b-5p and miR-30c-5p. (*A–D*) Validation of miR-30b-5p and miR-30c-5p overexpression and decreased *AVEN* expression by qRT-PCR. (**) *P*-value < 0.01, (***) *P*-value < 0.001, two-tailed Student's *t* test; n = 3 for each group. (*E*) Dual-luciferase reporter assay demonstrating the effects of miR-30b-5p and miR-30c-5p on the expression of the lengthened *AVEN* 3′ UTR (*AVEN*-L) in AC16 (*Left*) and 293T (*Right*) cells. (*) *P*-value < 0.05, (***) *P*-value < 0.001, two-tailed Student's *t* test; n = 4 for each group. (*F*) Mutation of the miR-30b-5p/miR-30c-5p binding site (seed sequence) predicted by TargetScan and verified by Sanger sequencing. (*G* and *H*) Dual-luciferase reporter assay demonstrating the effects of the mutated seed sequence within the lengthened *AVEN* 3′ UTR (*AVEN*-M). Co-transfections with either *AVEN*-L or *AVEN*-M and the miR-30b-5p/miR-30c-5p mimic or control in HEK293T cells. (***) *P*-value < 0.001, two-tailed Student's *t* test; n = 4 for each group.

upregulation of several CP factors may at least partially explain the global 3′ UTR lengthening that occurs after MI.

Knockdown of PABPN1 Promotes *AVEN* 3′ UTR Shortening and Partially Inhibits Cardiomyocytes Apoptosis. Next, the regulatory effects of CP factors on *AVEN* APA were investigated. As expected, *CPSF6* and *NUDT21* knockdown caused significant *AVEN* 3′ UTR shortening (*SI Appendix*, Fig. S11*F*). This was further confirmed by 3′ end sequencing after *CPSF6* knockdown in HEK293 cells (*SI Appendix*, Fig. S11*F*). For SRSF3, RNA-seq from HUVEC cell line revealed that its knockdown resulted in significant *AVEN* 3′ UTR shortening (*SI Appendix*, Fig. S11*G*). To validate the upstream regulators of *AVEN*, seven CP factors that were up-regulated in the MI mouse model were knocked down in both HEK293T and AC16 cells (*SI Appendix*, Fig. S11 *H* and *I*). Consistent with what was found in the public RNA-seq dataset, *CPSF6*, *PABPN1*, *NUDT21*, and *SRSF3* knockdown reduced *AVEN* distal poly(A) site usage in 293T cells and then resulted in 3′ UTR shortening (*SI Appendix*, Fig. S11*J*). In AC16 cells, *SRSF3* and *PABPN1* knockdown also reduced *AVEN* distal poly(A) site usage (Fig. 7*F*). Further experiments showed that knocking down PABPN1 promotes 3′ UTR shortening of *AVEN*, which in part upregulates AVEN expression (Fig. 7*G*). The upregulation of AVEN suppresses pro-apoptotic BAX protein levels (Fig. 7*H*), resulting in the inhibition of apoptosis in AC16 cells (*SI Appendix*, Fig. S11*K*, and Fig. 7*I*). We also confirmed that knocking down PABPN1 promotes upregulation of AVEN expression (Fig. 7 *J* and *K*) and a significant decrease in the BAX/BCL2 ratio in primary NRVMs (Fig. 7 *J* and *K*), indicating the pro-apoptotic effect of PABPN1. Taken together, these data suggest that the upregulation of PABPN1 after MI may promote *AVEN* 3′ UTR lengthening and exacerbate cardiomyocyte apoptosis.

Discussion

APA is a widespread, cotranscriptional regulatory mechanism for fine-tuning gene expression that is involved in diverse physiological and pathological processes. Here, with the RNA-seq data from both human ICM samples and an MI mouse model, we have revealed a global, APA-mediated 3′ UTR-lengthening pattern in response to myocardial ischemic injury. Additionally, we revealed that 3′ UTR lengthening of *AVEN* provides additional binding sites for miR-30b-5p/miR-30c-5p, thus leading to down-regulated *AVEN* expression. This in turn partially contributes to cardiomyocyte apoptosis, which plays a key role in the pathogenesis of MI and HF (*SI Appendix*, Fig. S12). Importantly, AAV9-mediated *AVEN* overexpression in cardiomyocytes ameliorates MI-induced cardiac remodeling and dysfunction. This study demonstrates the impact of APA in response to MI and to suggest the anti-apoptotic gene, *AVEN*, as a potential therapeutic target for treating post-MI HF.

In recent years, several studies have emphasized the importance of APA in the regulation of heart diseases, including dilated cardiomyopathy (DCM) and hypertrophic cardiomyopathy (HCM). APA dynamically changes in DCM, with a similar number of genes exhibiting 3′ UTR lengthening or shortening (37). However, in a mouse model of HCM, more genes have been shown to undergo 3′ UTR shortening than lengthening (38). Sudheesh et al. have also shown that NAD(P)H quinone dehydrogenase 1 APA plays a regulatory role in HCM (24). However, the dynamics and biological roles of APA in post-MI HF, a powerful mortality predictor, remain unclear. This study has revealed that more genes use distal poly(A) sites, leading to global 3′ UTR lengthening in post-MI HF. The three different global APA patterns corresponding to these three heart diseases demonstrate the complexity of APA regulation. Caused by acute blockage of the coronary artery, MI is commonly characterized by

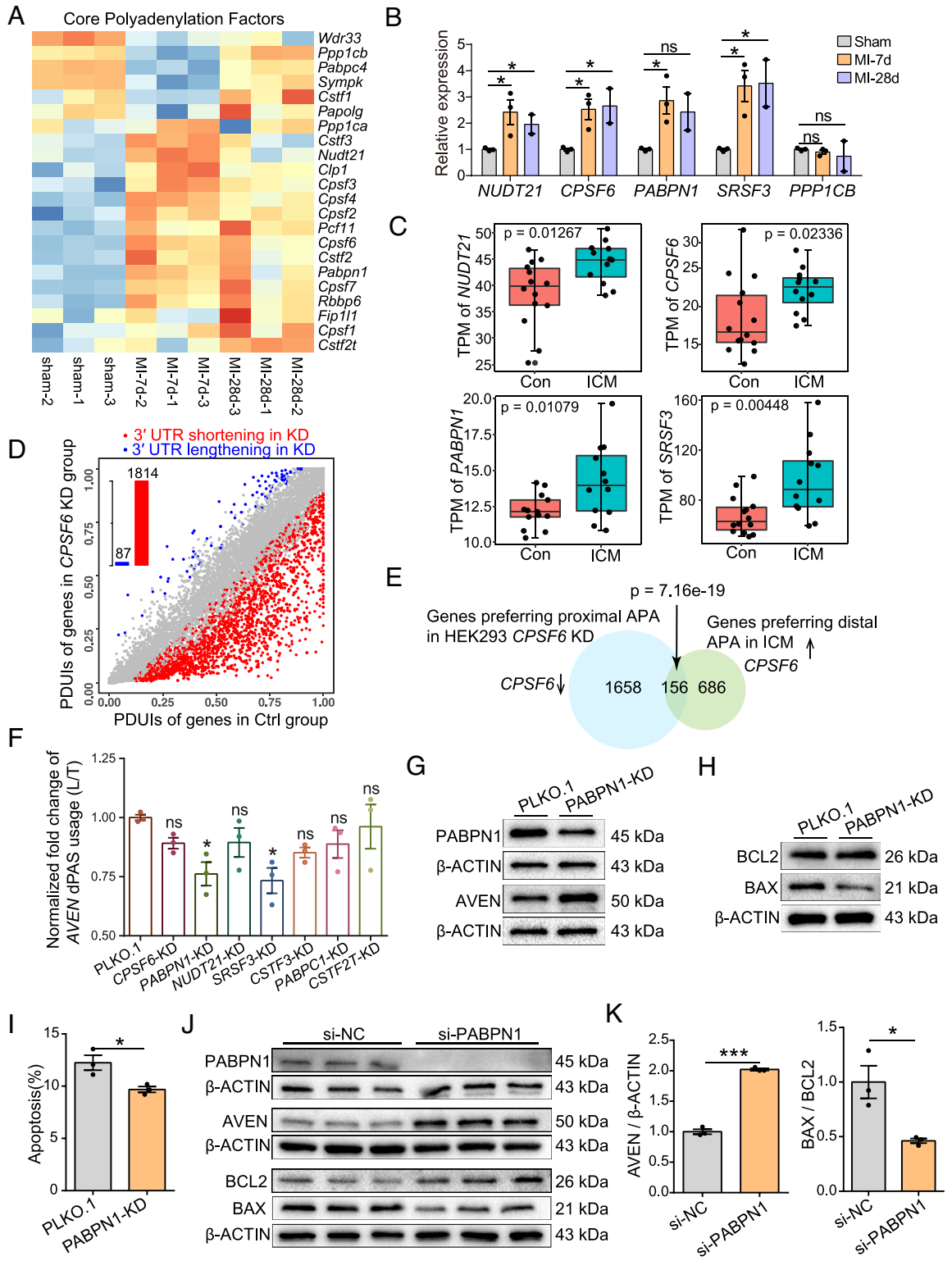

Fig. 7. A potential mechanism for APA regulation involves the upregulation of cleavage and polyadenylation factors after MI. (*A*) RNA-seq heatmap of core polyadenylation factors expressed in hearts from mice after MI or sham surgery. (*B*) Validation of the expression of five polyadenylation factors by qRT-PCR in the MI and sham groups. (∗) *P*-value < 0.05, two-tailed Student's *t* test; n = 3, 3, and 2, respectively. (*C*) TPM of four polyadenylation factors in human NF and ICM samples. The *P*-value was calculated based on a two-sided Wilcoxon rank-sum test; NF, n = 14; ICM, n = 13. (*D*) Scatterplot of PDUIs showing lengthened (n = 87) or shortened (n = 1,814) 3′ UTRs after *CPSF6* knockdown in HEK293 cells. FDR < 0.05, absolute ΔPDUIs ≥ 0.1 between control and *CPSF6*-knockdown cells are colored. (*E*) Venn diagram of genes with distal APA in ICM with higher *CPSF6* expression compared with genes with proximal APA in HEK293 cells with *CPSF6* knockdown. *P*-value, Fisher's exact test. (*F*) Validation of *AVEN* distal poly(A) site usage (ratio between long/total isoform, L/T) by qRT-PCR after knockdown of seven polyadenylation factors in AC16 cells. (ns) not significant, (∗) *P* - value < 0.05, one-way ANOVA; n = 3 for each group. (*G*) Western blot of PABPN1, AVEN protein levels before (PLKO.1) and after PABPN1 knockdown (PABPN1-KD) in AC16 cells. Internal control, β-ACTIN. (*H*) Western blot of BCL2, BAX protein levels before (PLKO.1) and after PABPN1 knockdown (PABPN1-KD) in AC16 cells. Internal control, β-ACTIN. (*I*) Quantification of flow cytometry analysis using annexin V and propidium iodide double-staining to assess apoptosis in PABPN1 knockdown AC16 cells. (∗) *P*-value < 0.05, two-tailed Student's *t* test; n = 3 for each group. (*J*) Western blot of PABPN1, AVEN, BAX, and BCL2 protein levels before (si-NC) and after PABPN1 knockdown (si-PABPN1) in NRVMs. Internal control, β-ACTIN. (*K*) Quantification of *J*. (∗) *P*-value < 0.05, (∗∗∗) *P*-value < 0.001, two-tailed Student's *t* test; n = 3 for each group.

prolonged inflammation, cardiomyocyte death, and subsequent extracellular matrix deposition. Differences in the pathophysiological processes of MI and other cardiomyopathies may lead to the dysregulation of various CP factors, ultimately causing different patterns of 3′ UTR changes. Therefore, future studies focusing on these dynamic changes and roles of APA in the pathological processes of different heart diseases are warranted.

AVEN is an intracellular apoptosis inhibitor that interacts with B-cell lymphoma-extra large and apoptotic protease activating factor 1 (30). It has also been reported to play an oncogenic role in multiple cancers (32, 39). However, AVEN remains less studied in the cardiovascular field. AVEN has been shown to suppress macrophage apoptosis and promote the progression of atherosclerosis (40). Zhang et al. have found that miR-30b-5p promotes cardiomyocyte apoptosis after hypoxia-induced injury by targeting *AVEN* (41). Chau et al. demonstrated that AVEN interacts with BCL-2 family proteins (30), which have been shown to reduce myocardial reperfusion injury and improve cardiac function (42, 43). In this study, *AVEN* overexpression increases BCL-2 protein levels and protects the injured heart from dysfunction after MI (Fig. 5 and *SI Appendix*, Fig. S9). Moreover, our findings have revealed *AVEN* dysregulation at the APA level in both ICM patient samples and an MI mouse model, and targeting this gene may represent a potential strategy for treating post-MI HF. In addition, besides the fraction of genes with altered steady-state mRNA levels (like *AVEN*), there is also a large proportion of APA-altered genes whose expression is not significantly changed (*SI Appendix*, Fig. S3*A*), which is consistent with findings in other systems (44, 45). We intend to integrate protein profiling data to identify APA-regulated genes with unchanged RNA levels but significantly altered protein levels and investigate their role in ischemic HF. Furthermore, genes for which APA does not affect expression but does affect protein localization are very interesting and warrant further investigation.

CRISPR-iPAS has been reported to modulate APA by recruiting dead Cas13 (dCas13) to the proximal or distal poly(A) signal, thereby blocking the binding of CP factors to cis-elements and interfering with APA (46). To directly verify whether interferences APA of *AVEN* could regulate cellular apoptosis, we designed three sgRNAs targeting the proximal poly(A) signal and two sgRNAs targeting the distal poly(A) signal of *AVEN* (*SI Appendix*, Fig. S13*A*). We conducted interferences in both AC16 and HEK293T cells. However, the dCas13 plasmid is too large (over 13 kb) and its transfection efficiency is very low in AC16 cells (*SI Appendix*, Fig. S13 *B* and *C*). Therefore, we performed APA interferences in HEK293T cells, which have a higher transfection efficiency (*SI Appendix*, Fig. S13*B*). Our results showed that the two sgRNAs (g4 and g5) targeting the distal poly(A) signal were unable to suppress the poly(A) site usage (*SI Appendix*, Fig. S13 *D* and *E*), whereas the sgRNA-3 (g3) targeting the proximal poly(A) site partially represses its usage (*SI Appendix*, Fig. S13*F*), promoting 3′ UTR lengthening of *AVEN* (*SI Appendix*, Fig. S13*G*). Furthermore, the 3′ UTR lengthening of *AVEN* due to perturbation of g3 down-regulated its expression (*SI Appendix*, Fig. S13 *H* and *I*), which partially reduced cell viability (*SI Appendix*, Fig. S13*J*) and increased cellular apoptosis in HEK293T cells (*SI Appendix*, Fig. S13 *K* and *L*). These results hinted that 3′ UTR lengthening of *AVEN* could partially downregulate its expression, which is known to promote cellular apoptosis. CRISPR-iPAS manipulated APA of *AVEN* by approximately 20% switch of proximal and distal PA site, while in human ischemic HF, *AVEN* has a 36% increase in distal PA site usage. To manipulate APA of *AVEN*, we also tried other previously reported strategies: CRISPR-cas9 (47) and CRISPRpas (48). For CRISPR-cas9, we designed four sgRNAs targeting the distal poly(A) signal and its upstream regions and one sgRNA targeting the proximal poly(A) signal (*SI Appendix*, Fig. S14*A*). However, genomic DNA amplification and subsequent Sanger sequencing showed that only two sgRNAs (d-g1 and d-g2) successfully induced a deletion or mutation upstream of the *AVEN* distal PAS (*SI Appendix*, Fig. S14*B*), but APA of *AVEN* was not affected by these manipulations (*SI Appendix*, Fig. S14*C*), possibly because that the PAS was not disrupted. For CRISPRpas, we used *TIMP2* from CRISPRpas article as a positive control, which successfully promoted the usage of the proximal PA site and up-regulated its expression (*SI Appendix*, Fig. S15 *A* and *B*), demonstrating the effectiveness of this tool. We then designed three sgRNAs for APA manipulation of *AVEN*, but unfortunately, they failed to manipulate APA of *AVEN* in both HEK293T and AC16 cell lines (*SI Appendix*, Fig. S15*C*). Further analysis of the CRISPRpas article revealed that the sgRNAs with target sites close to the proximal PA site (within 200 nt) could not elicit APA changes. Given that the alternative 3′ UTR of *AVEN* is very short (230 nt), the designed gRNAs were all located close to the proximal PA site, making it difficult to elicit APA changes. In the future, by improving the efficiency of manipulating APA of *AVEN*, we believe manipulating APA of *AVEN* might present more impact on targeting the cell apoptosis phenotype.

Another important question regarding APA in ICM relates to the mechanism of altered poly(A) site usage. APA involves complex and precise regulation. A growing number of APA-regulatory factors have been identified and characterized in the past few years, including four protein complexes (CPSF, CSTF, CFI, and CFII) and several single proteins (PAP, RBBP6, and PABPN1) (10). Some of these proteins have global effects on APA, whereas others only affect APA within specific genes. This study has revealed that core CP factors are differentially expressed in an MI mouse model. Furthermore, four APA-regulatory factors (NUDT21, CPSF6, PABPN1, and SRSF3) may contribute to the global 3′ UTR lengthening that occurs in ICM (Fig. 7). This observation is consistent with the previous studies showing that these four APA-regulatory factors promote distal poly(A) site selection or inhibit proximal poly(A) site usage, thus regulating 3′ UTR lengthening (10, 33, 34, 49). Additionally, we found that the upregulation of PABPN1 after MI may promote *AVEN* 3′ UTR lengthening and exacerbate cardiomyocyte apoptosis. APA regulation is complex and involves many factors, including Pol II elongation and termination, CPA factors, splicing factors, promoters, and enhancers (44). Further investigation is needed to determine the potential upstream factors responsible for the global 3′ UTR lengthening observed in ischemic HF.

In summary, we have revealed a global 3′ UTR lengthening pattern after MI. Sufficient AVEN expression is critical after MI; however, APA-mediated *AVEN* 3′ UTR lengthening contributes to its downregulation. AVEN knockdown increased cardiomyocyte apoptosis. Therefore, our data have not only revealed APA as a unique regulatory mechanism for gene expression after MI but have also indicated AVEN as a critical cardioprotective target after MI.

Materials and Methods

Please see *SI Appendix, Materials and Methods* for a full description of the methods used.

Human Subjects. LV samples were obtained from patients with ischemic HF and healthy subjects. All patients provided written informed consent. All procedures performed in this study were approved by the Zhongshan Hospital, Fudan University, Review Board (B2022-267R) and conformed to the Declaration of Helsinki. To explore human HF, we obtained human LV samples from the heart at the time of transplantation. Subjects were grouped as control group (noncardiac causes of death, including car accident or trauma) or ICM group. Patients receiving chemotherapy or radiation therapy were excluded.

RNA-seq Data Analyze. Raw data reads quality was checked by Fastqc and then aligned to the human reference genome sequence (UCSC hg19 assembly) using STAR (50), and the uniquely mapped reads were assigned to genomic features using featureCounts (51). Differential gene expression analysis was performed using DESeq2 (52) with a statistical cutoff of FDR (False discovery rate) < 0.05 and fold change > 1.5. The enrichment analysis was performed by clusterProfiler (53). The mouse MI model RNA-seq was treated with the same procedure as human data, and it was aligned to the mouse genome (version mm10).

For APA analysis, DaPars (28) was used to de novo identification of dynamic APAs from standard RNA-seq, and the resulted PDUI value was used to indicate the percentage of transcripts using the distal poly(A) site.

The APAatlas (27) is a database that utilizes RNA-seq data from the Genotype-Tissue Expression (54) project to analyze APA events in human tissues. We obtained the PDUIs for human ischemic LV samples from the APAatlas database and used them for further analysis.

Data, Materials, and Software Availability. All raw and processed sequencing data generated in this study have been submitted to the Gene Expression Omnibus (GEO) under accession number GSE236374 (55). Other publicly available raw sequencing data of RNA-seq were obtained from NCBI under the accession numbers: GSE116250 (25), GSE179630 (33), and PRJNA523954 (35) (BioProject accession number). All study data are included in the article and/or *SI Appendix*.

ACKNOWLEDGMENTS. We sincerely thank Dr. Wei Chen (School of Life Sciences, Southern University of Science and Technology) for sharing the plasmids used to express dCas13 proteins and gRNA. This work was supported by the National Natural Science Foundation of China (82130010 to A.S. and 92249302, 91949107 to T.N.), National Science Fund for Distinguished Young Scholars (81725002), the National Key R&D Program of China (2021YFA0909300), the Basic research projects of Shanghai Science and Technology Commission (22JC1400500), and the Innovation Program of Shanghai Municipal Education Commission.

Author affiliations: [a]State Key Laboratory of Genetic Engineering, Human Phenome Institute, Department of Anthropology and Human Genetics, School of Life Sciences and Zhongshan Hospital, Fudan University, Shanghai 200438, China; [b]Department of Cardiology, Zhongshan Hospital, Fudan University, Shanghai 200032, China; [c]Shanghai Institute of Cardiovascular Diseases, Zhongshan Hospital, Shanghai 200032, China; [d]National Clinical Research Center for Aging and Medicine, Huashan Hospital, Fudan University, Shanghai 200040, China; [e]State key Laboratory of Reproductive Regulation and Breeding of Grassland Livestock, Institutes of Biomedical Sciences, School of Life Sciences, Inner Mongolia University, Hohhot 010021, China; and [f]Zhangjiang Fudan International Innovation Center, Fudan University, Shanghai 201203, China

1. J. L. Anderson, D. A. Morrow, Acute myocardial infarction. *N. Engl. J. Med.* **376**, 2053–2064 (2017).
2. I. M. Seropian, S. Toldo, B. W. Van Tassell, A. Abbate, Anti-inflammatory strategies for ventricular remodeling following ST-segment elevation acute myocardial infarction. *J. Am. Coll. Cardiol.* **63**, 1593–1603 (2014).
3. R. G. de Bruin, T. J. Rabelink, A. J. van Zonneveld, E. P. van der Veer, Emerging roles for RNA-binding proteins as effectors and regulators of cardiovascular disease. *Eur. Heart J.* **38**, 1380–1388d (2017).
4. M. M. van den Hoogenhof, Y. M. Pinto, E. E. Creemers, R. N. A. Splicing, Regulation and dysregulation in the heart. *Circ. Res.* **118**, 454–468 (2016).
5. W. Guo *et al.*, RBM20, a gene for hereditary cardiomyopathy, regulates titin splicing. *Nat. Med.* **18**, 766–773 (2012).
6. D. C. Di Giammartino, K. Nishida, J. L. Manley, Mechanisms and consequences of alternative polyadenylation. *Mol. Cell* **43**, 853–866 (2011).
7. A. Derti *et al.*, A quantitative atlas of polyadenylation in five mammals. *Genome Res.* **22**, 1173–1183 (2012).
8. G. Edwalds-Gilbert, K. L. Veraldi, C. Milcarek, Alternative poly(A) site selection in complex transcription units: Means to an end? *Nucleic Acids Res.* **25**, 2547–2561 (1997).
9. Z. Zhao *et al.*, Cancer-associated dynamics and potential regulators of intronic polyadenylation revealed by IPAFinder using standard RNA-seq data. *Genome Res.* **31**, 2095–2106 (2021).
10. B. Tian, J. L. Manley, Alternative polyadenylation of mRNA precursors. *Nat. Rev. Mol. Cell Biol.* **18**, 18–30 (2017).
11. C. Mayr, D. P. Bartel, Widespread shortening of 3′UTRs by alternative cleavage and polyadenylation activates oncogenes in cancer cells. *Cell* **138**, 673–684 (2009).
12. R. Sandberg, J. R. Neilson, A. Sarma, P. A. Sharp, C. B. Burge, Proliferating cells express mRNAs with shortened 3′ untranslated regions and fewer microRNA target sites. *Science* **320**, 1643–1647 (2008).
13. S. N. Floor, J. A. Doudna, Tunable protein synthesis by transcript isoforms in human cells. *Elife* **5**, e10921 (2016).
14. L. L. Chen, G. G. Carmichael, Altered nuclear retention of mRNAs containing inverted repeats in human embryonic stem cells: Functional role of a nuclear noncoding RNA. *Mol. Cell* **35**, 467–478 (2009).
15. J. Neve *et al.*, Subcellular RNA profiling links splicing and nuclear DICER1 to alternative cleavage and polyadenylation. *Genome Res.* **26**, 24–35 (2016).
16. B. D. Berkovits, C. Mayr, Alternative 3′ UTRs act as scaffolds to regulate membrane protein localization. *Nature* **522**, 363–367 (2015).
17. R. Elkon *et al.*, E2F mediates enhanced alternative polyadenylation in proliferation. *Genome Biol.* **13**, R59 (2012).
18. M. Chen *et al.*, 3′ UTR lengthening as a novel mechanism in regulating cellular senescence. *Genome Res.* **28**, 285–294 (2018), 10.1101/gr.224451.117.
19. Z. Ji, J. Y. Lee, Z. H. Pan, B. J. Jiang, B. Tian, Progressive lengthening of 3′ untranslated regions of mRNAs by alternative polyadenylation during mouse embryonic development. *Proc. Natl. Acad. Sci. U.S.A.* **106**, 7028–7033 (2009).
20. X. Jia *et al.*, The role of alternative polyadenylation in the antiviral innate immune response. *Nat. Commun.* **8**, 14605 (2017).
21. Z. Xia *et al.*, Dynamic analyses of alternative polyadenylation from RNA-seq reveal a 3′-UTR landscape across seven tumour types. *Nat. Commun.* **5**, 5274 (2014).
22. Y. G. Fu *et al.*, Differential genome-wide profiling of tandem 3′ UTRs among human breast cancer and normal cells by high-throughput sequencing. *Genome Res.* **21**, 741–747 (2011).
23. N. Mohan, V. Kumar, D. T. Kandala, C. C. Kartha, R. S. Laishram, A splicing-independent function of RBM10 controls specific 3′ UTR processing to regulate cardiac hypertrophy. *Cell Rep.* **24**, 3539–3553 (2018).
24. A. P. Sudheesh, N. Mohan, N. Francis, R. S. Laishram, R. A. Anderson, Star-PAP controlled alternative polyadenylation coupled poly(A) tail length regulates protein expression in hypertrophic heart. *Nucleic Acids Res.* **47**, 10771–10787 (2019).
25. M. E. Sweet *et al.*, Transcriptome analysis of human heart failure reveals dysregulated cell adhesion in dilated cardiomyopathy and activated immune pathways in ischemic heart failure. *BMC Genom.* **19**, 812 (2018).
26. T. L. Bailey *et al.*, MEME SUITE: Tools for motif discovery and searching. *Nucleic Acids Res.* **37**, W202–W208 (2009).
27. W. Hong *et al.*, APAatlas: Decoding alternative polyadenylation across human tissues. *Nucleic Acids Res.* **48**, D34–D39 (2020).
28. V. P. M. van Empel *et al.*, Myocyte apoptosis in heart failure. *Cardiovasc Res.* **67**, 21–29 (2005).
29. D. Wencker *et al.*, A mechanistic role for cardiac myocyte apoptosis in heart failure. *J. Clin. Invest.* **111**, 1497–1504 (2003).
30. B. N. Chau, E. H. Cheng, D. A. Kerr, J. M. Hardwick, Aven, a novel inhibitor of caspase activation, binds Bcl-xL and Apaf-1. *Mol. Cell* **6**, 31–40 (2000).
31. Z. Baranski *et al.*, Aven-mediated checkpoint kinase control regulates proliferation and resistance to chemotherapy in osteosarcoma cells. *Cancer Res.* **75** (2015).
32. M. Eissmann *et al.*, Overexpression of the anti-apoptotic protein AVEN contributes to increased malignancy in hematopoietic neoplasms. *Oncogene* **32**, 2586–2591 (2013).
33. S. Ghosh *et al.*, CFIm-mediated alternative polyadenylation remodels cellular signaling and miRNA biogenesis. *Nucleic Acids Res.* **50**, 3096–3114 (2022).
34. O. D. Schwich *et al.*, SRSF3 and SRSF7 modulate 3′ UTR length through suppression or activation of proximal polyadenylation sites and regulation of CFIm levels. *Genome Biol.* **22**, 82 (2021).
35. T. Shen *et al.*, Alternative polyadenylation dependent function of splicing factor SRSF3 contributes to cellular senescence. *Aging (Albany NY)* **11**, 1356–1388 (2019).
36. W. C. Li *et al.*, Systematic profiling of Poly(A) plus transcripts modulated by core 3′ end processing and splicing factors reveals regulatory rules of alternative cleavage and polyadenylation. *Plos Genet.* **11**, e1005166 (2015).
37. E. E. Creemers *et al.*, Genome-wide polyadenylation maps reveal dynamic mRNA 3′-end formation in the failing human heart. *Circ. Res.* **118**, 433–438 (2016).
38. J. Y. Park *et al.*, Comparative analysis of mRNA isoform expression in cardiac hypertrophy and development reveals multiple post-transcriptional regulatory modules. *PLoS One* **6**, e22391 (2011).
39. Z. Baranski *et al.*, Aven-mediated checkpoint kinase control regulates proliferation and resistance to chemotherapy in conventional osteosarcoma. *J. Pathol.* **236**, 348–359 (2015).
40. W. Huan *et al.*, YKL-40 aggravates early-stage atherosclerosis by inhibiting macrophage apoptosis in an aven-dependent way. *Front. Cell Dev. Biol.* **9**, 752773 (2021).
41. L. F. Zhang, X. W. Jia, Down-regulation of miR-30b-5p protects cardiomyocytes against hypoxia-induced injury by targeting Aven. *Cell Mol. Biol. Lett.* **24**, 61 (2019).
42. V. Brocheriou *et al.*, Cardiac functional improvement by a human Bcl-2 transgene in a mouse model of ischemia/reperfusion injury. *J. Gene. Med.* **2**, 326–333 (2000).
43. Z. Chen, C. C. Chua, Y. S. Ho, R. C. Hamdy, B. H. Chua, Overexpression of Bcl-2 attenuates apoptosis and protects against myocardial I/R injury in transgenic mice. *Am. J. Physiol. Heart Circ. Physiol.* **280**, H2313–H2320 (2001).
44. S. Mitschka, C. Mayr, Context-specific regulation and function of mRNA alternative polyadenylation. *Nat. Rev. Mol. Cell Biol.* **23**, 779–796 (2022).
45. N. Spies, C. B. Burge, D. P. Bartel, 3′ UTR-isoform choice has limited influence on the stability and translational efficiency of most mRNAs in mouse fibroblasts. *Genome Res.* **23**, 2078–2090 (2013).
46. S. Tian *et al.*, CRISPR-iPAS: A novel dCAS13-based method for alternative polyadenylation interference. *Nucleic Acids Res.* **50**, e26 (2022).
47. J. Wang *et al.*, Comprehensive mapping of alternative polyadenylation site usage and its dynamics at single-cell resolution. *Proc. Natl. Acad. Sci. U.S.A.* **119**, e2113504119 (2022).
48. J. Shin *et al.*, CRISPRpas: Programmable regulation of alternative polyadenylation by dCas9. *Nucleic Acids Res.* **50**, e25 (2022).
49. C. P. Masamha *et al.*, CFIm25 links alternative polyadenylation to glioblastoma tumour suppression. *Nature* **510**, 412–416 (2014).
50. A. Dobin *et al.*, STAR: Ultrafast universal RNA-seq aligner. *Bioinformatics* **29**, 15–21 (2013).
51. Y. Liao, G. K. Smyth, W. Shi, featureCounts: An efficient general purpose program for assigning sequence reads to genomic features. *Bioinformatics* **30**, 923–930 (2014).
52. M. I. Love, W. Huber, S. Anders, Moderated estimation of fold change and dispersion for RNA-seq data with DESeq2. *Genome Biol.* **15**, 550 (2014).
53. G. Yu, L. G. Wang, Y. Han, Q. Y. He, clusterProfiler: An R package for comparing biological themes among gene clusters. *OMICS* **16**, 284–287 (2012).
54. G. T. Consortium, The GTEx Consortium atlas of genetic regulatory effects across human tissues. *Science* **369**, 1318–1330 (2020).
55. S. Song, P. Yu, X. Zhang, A. Sun, Bulk RNA-seq of mouse heart tissue for analyzing gene expression of myocardial infarction progression. NCBI Gene Expression Omnibus (GEO). https://www.ncbi.nlm.nih.gov/geo/query/acc.cgi?acc=GSE236374. Deposited 4 July 2023.